

Detailed Fault Structure of the 2000 Western Tottori, Japan, Earthquake Sequence

by Eiichi Fukuyama, William L. Ellsworth, Felix Waldhauser, and Atsuki Kubo

Abstract We investigate the faulting process of the aftershock region of the 2000 western Tottori earthquake (M_w 6.6) by combining aftershock hypocenters and moment tensor solutions. Aftershock locations were precisely determined by the double difference method using P - and S -phase arrival data of the Japan Meteorological Agency unified catalog. By combining the relocated hypocenters and moment tensor solutions of aftershocks by broadband waveform inversion of FREESIA (F-net), we successfully resolved very detailed fault structures activated by the mainshock. The estimated fault model resolves 15 individual fault segments that are consistent with both aftershock distribution and focal mechanism solutions. Rupture in the mainshock was principally confined to the three fault elements in the southern half of the zone, which is also where the earliest aftershocks concentrate. With time, the northern part of the zone becomes activated, which is also reflected in the postseismic deformation field. From the stress tensor analysis of aftershock focal mechanisms, we found a rather uniform stress field in the aftershock region, although fault strikes were scattered. The maximum stress direction is N107°E, which is consistent with the tectonic stress field in this region. In the northern part of the fault, where no slip occurred during the mainshock but postseismic slip was observed, the maximum stress direction of N130°E was possible as an alternative solution of stress tensor inversion.

Introduction

On 6 October 2000 at 04:30 UTC, the western Tottori earthquake (M_w 6.6) occurred in southwestern Japan, where very few large earthquakes have occurred since the 1943 Tottori earthquake of M 7.4 (Kanamori, 1972) (Fig. 1).

Within the 15 years before the 2000 western Tottori earthquake, background seismicity covered the whole aftershock region of the 2000 western Tottori earthquake and several M 5 earthquakes were observed on the mainshock fault of the 2000 western Tottori earthquake (southern part of the aftershock region) (Shibutani et al., 2002). At that time, since the seismic observation network was sparse, they could not obtain the precise geometry of the fault structure in this region. But from the background seismicity, a very vague image of the fault could be obtained before the mainshock. Their result showed that in the southern part of the aftershock region of the western Tottori earthquake, a fault existed before the mainshock but in the northern part, there was no information about the geometry of the fault before the mainshock.

Moreover, Yagi and Kikuchi (2000) and Iwata and Sekiguchi (2001) analyzed the rupture process of the 2000 western Tottori earthquake, and they found that slip occurred only in the southern part of the aftershock region. Sagiya

et al. (2002) reported from the analysis of Global Positioning System (GPS) data that the postseismic slip occurred in the northern part of the aftershock region where little slip occurred during the mainshock.

In the western Tottori region, northwest-southeast tectonic loading is dominant (Tsukahara and Kobayashi, 1991) due to the subduction of both the Pacific and Philippine sea plates beneath the Eurasia plate. This is the typical stress environment in the southwest of Japan (Ichikawa, 1971). Due to this driving stress, north-south- or east-west-trending strike-slip faults are commonly observed (Research Group for Active Faults of Japan, 1991).

The western Tottori earthquake and its aftershocks occurred within the recently developed nationwide seismic network. High-quality seismic data were available from the microearthquake networks operated by Hi-net, the Japan Meteorological Agency (JMA), and universities. Broadband waveforms from the FREESIA (now called F-net) broadband seismic network and strong motion waveforms from the K-net and Kik-net are also available. JMA routinely processes the microearthquake data from Hi-net, the university group network, and its own network (Japan Meteorological Agency, 2001). JMA produced the unified data set of phase

arrival times of the Tottori mainshock and its aftershocks that we used in this study. The National Research Institute for Earth Science and Disaster Prevention (NIED) routinely estimates the seismic moment tensors whose JMA magnitudes are greater than 3.5 using the FREESIA network (Fukuyama *et al.*, 1998, 2001a; Kubo *et al.*, 2002).

A new high-resolution hypocenter relocation technique has recently been developed by Waldhauser and Ellsworth (2000). This technique minimizes the residuals between observed and calculated travel time differences (or double differences [DDs]) for pairs of nearby earthquakes. By forming differences in this manner, the common mode travel time errors are canceled, making the computation insensitive to the assumed velocity structure. We have applied this method to the 2000 western Tottori earthquake and its aftershocks.

In this article, in order to reveal the detailed fault structure in the region of the 2000 western Tottori earthquake, we first relocated its aftershocks using the DD method. Then, we compared the fault structure revealed by the relocated seismicity with the moment tensors obtained from broadband seismic waveforms of the corresponding events. We construct a fault model of the 2000 western Tottori earthquake region based on the relocated aftershock hypocenters and moment tensor solutions. Finally we estimate the stress field using stress tensor inversion and investigate its compatibility with the fault geometry.

Relocation of Aftershock Sequence

JMA gathers all the data streams from the microearthquake stations of Hi-net, several university networks, and its own network and routinely reads the *P*- and *S*-wave arrivals to determine the hypocenters (Japan Meteorological Agency, 2001). We used this arrival time data for earthquakes occurring from 6 October to 17 November 2000, in the region between 35.00° and 35.50° N, 133.00° and 133.55° E. In total, there are about 9200 events in the JMA unified data set, and we successfully relocated about 8500 using the DD method.

To relocate the earthquakes with “hypo DD” (a program for the DD method; Waldhauser and Ellsworth, 2000), we used stations within an epicentral distance of 120 km (Fig. 1) in order to exclude the *Pn* arrivals. We discarded events with fewer than eight readings. We used a velocity structure with four layers, as shown in Table 1. The *S*-wave velocity is assumed to be $1/\sqrt{3}$ of the *P*-wave speed.

We also tested the velocity model used for routine location at the Disaster Prevention Research Institute, Kyoto University (T. Shibutani, personal comm. 2000), which also consists of four layers (Table 1). The main difference between the models is the velocity in the shallow parts. However, there are no distinct differences in the seismicity pattern. This implies that the DD method is robust with respect to the uncertainties in the velocity structure. We prefer the primary model because fewer events were pushed above the

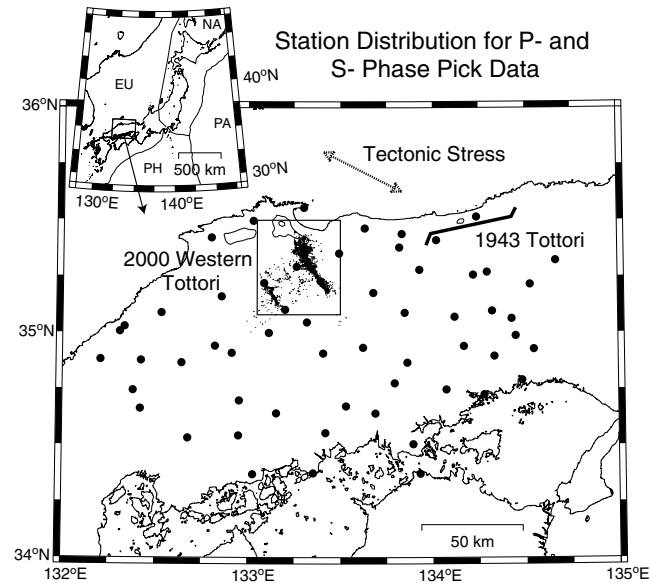


Figure 1. Station distribution of high-gain microseismic network in western Honshu, Japan, used for the relocation. Stations belong to either Hi-net, university network, or the JMA network. The epicentral distribution of the 2000 western Tottori aftershocks and fault trace of the 1943 Tottori earthquakes are also shown. In upper left panel, the configuration of the plates in this region is shown. EU, Eurasian plate; NA, North American plate; PA, Pacific plate; PH, Philippine Sea plate.

Table 1
Velocity Structure

This Study		Kyoto University	
Depth (km)	<i>P</i> -Wave Velocity (km/sec)	Depth (km)	<i>P</i> -Wave Velocity (km/sec)
0.0	3.0	0.0	5.5
1.0	4.0	2.0	6.05
3.0	6.0	16.0	6.6
30.0	8.0	38.0	8.0

model surface, indicating that low velocity near the surface is more appropriate in this case.

Included among the unrelocated earthquakes are fewer than 10 *M* 3–4 earthquakes that occurred within 1/2 hour of the mainshock. Relocation failed because of an insufficient number of readings created by their overlapping waveforms. All other unrelocated aftershocks are all *M* 2 or smaller earthquakes. The percentages of unrelocated events for greater than and less than *M* 3.0 events are 2.1% and 6.6%, respectively. Thus we could successfully relocate most of the important aftershocks.

In Figure 2, the original JMA hypocenters from the unified catalog and the result of the DD relocation are shown. Many fine fault structures that are suggested in the JMA hypocenters can be easily recognized in the DD relocations. In the gross view, two major fault trends are evident. One

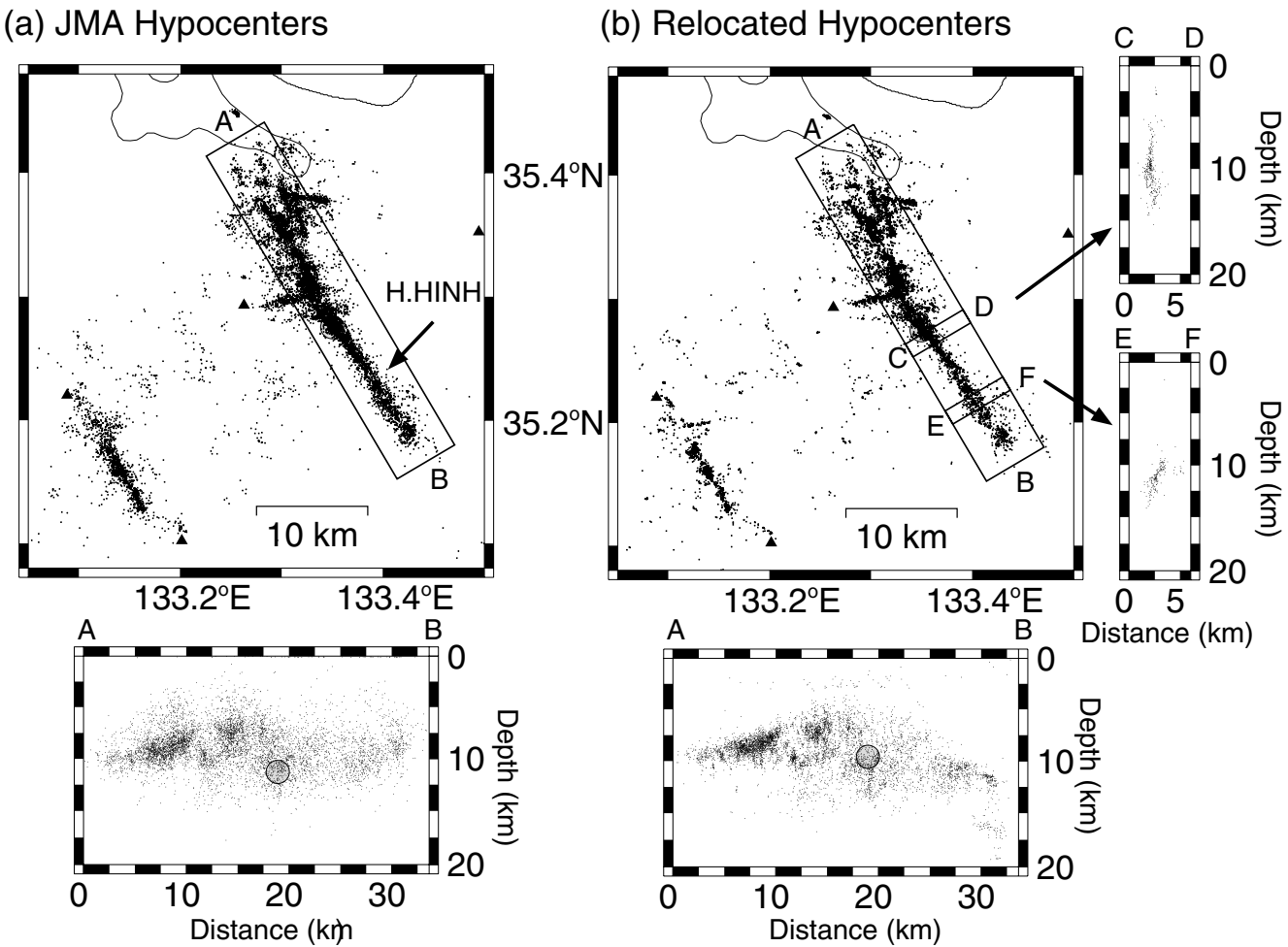


Figure 2. (a) Original distribution of aftershocks estimated by JMA. (b) Distribution of aftershocks relocated by the double difference method. All the earthquakes are plotted with a fixed scale in order to enhance the lineament of the fault trace. The gray circle shows the mainshock hypocenter. Triangles indicate the station locations. Station H.HINH was used to examine the depths of earthquakes. The AB box in both figures shows the longitudinal cross section of hypocenters. The CD and EF cross sections are also shown for relocated hypocenters.

trends N145°E, which is consistent with the mainshock fault direction. The other is almost north–south (N170°E) in trend, which can be seen in the northern part. It should also be noted that there are conjugate faults for both groups, the western branch and northern fault group. These two lineaments (N145°E and N170°E) might suggest a pre-existing fault system at depth 8–10 km.

In Figure 2, a longitudinal cross section of relocated hypocenters is shown. Aftershocks in the southern region (12–30 km in distance in Fig. 2), where slip occurred during the mainshock (Yagi and Kikuchi, 2000; Iwata and Sekiguchi, 2001), are distributed from 2 to 15 km in depth; however, in the northern part (0–12 km in distance in Fig. 2) where little if any slip occurred during the mainshock, aftershocks are distributed in a very narrow depth range. Toward the southern end of the zone, the fault plane develops a westward dip (Fig. 2).

The sparse geometry of the permanent station network limits our ability to determine focal depths, particularly for the shallowest event. Only two permanent stations are located close to the main body of the aftershock zone, and none atop the complex northern end of the zone. Consequently, our depths in this region are poorly constrained. Focal depths estimated using more than 60 temporary stations installed just above the focal region by the Joint Group for Dense Aftershock Observation of the 2000 Tottori-ken Seibu Earthquake (2001) were reported to be as shallow as 2 km in the northern part. We believe that their focal depths should be more accurate than ours. Fortunately, the vast majority of the structures observed in the northern part of the zone are vertical strike-slip faults, and thus the lack of absolute depth control little affects their interpretation.

In the southern part of the zone, one permanent station sits just above the fault (H.HINH; see Fig. 2). We can ex-

amine the depth of earthquakes occurring beneath this station using $S-P$ times. Figure 3 shows the relation between estimated depths and observed $S-P$ times for earthquakes occurring within the epicentral distance of 2 km from this station. There are some earthquakes that appear to be systematically too deep, but others agree with the observed $S-P$ interval. In this figure, $S-P$ times in the range from 0.4 to 1.8 sec correspond to the depth interval from 3.2 to 14.8 km, assuming that the average $V_p = 6$ km/sec and all earthquakes occur beneath the station (i.e., $\Delta = 0$ km). The depth range of the relocation is 4–15 km, which is consistent with the estimates using $S-P$ times. These depths are also consistent with the depth range of the rupture during the mainshock (2 and 15 km) estimated by waveform inversion of near-field accelerograms (Iwata and Sekiguchi, 2001).

In Figure 4, the temporal development of the cumulative aftershock distribution is shown. Within 15 min of the mainshock, the aftershocks concentrate along the southern part, where the slip during the mainshock is estimated to occur (e.g., Yagi and Kikuchi, 2000; Iwata and Sekiguchi, 2001). By 60 min after the mainshock, activity appears throughout the entire extent of the aftershock region. As time progresses, activity fills in the fault structures.

On 8 October at 13:17, the largest aftershock (M_w 5.1) occurred about 20 km west of the mainshock region. This event was followed by its own aftershocks. With additional passage of time, the structures within the main zone densified and widened, which might suggest that the aftershock activity expanded from the mainshock fault surface to the entire fault zone. Also, several new alignments of aftershocks were recognized inside the aftershock region.

As stated before, there are about 10 relatively large earthquakes ($M > 2$) that occurred within 30 min after the mainshock and could not be relocated, but other unrelocated earthquakes are all very small earthquakes ($M < 2$). Thus

while the first snapshot in Figure 4 is missing about 10 detected earthquakes, the other snapshots will not change significantly since the total number of unrelocated earthquakes is only 6.4%.

Fault Model by Aftershocks and Moment Tensors

In Figure 5, strike directions and moment tensor solutions for $M \geq 3.5$ aftershocks are displayed together with all relocated hypocenters. All focal mechanism parameters are listed in Table 2. The strike directions are estimated from the moment tensor analysis using broadband seismic waveforms (Fukuyama *et al.*, 1998, 2001a). The details of the procedure can also be found in Fukuyama and Dreger (2000), Fukuyama *et al.* (2001b), and Kubo *et al.* (2002). Among the two possible fault planes in the moment tensor solution, the fault plane was chosen in the following way. First, the direction close to that of the mainshock rupture (N150°E) is chosen. The provisional plane is then compared to the fault trend of the DD hypocenters, and obvious disagreements are manually switched to the auxiliary plane.

According to Kubo *et al.* (2002), errors in principal axis directions are less than 15° in the NIED seismic moment tensor catalog. This error estimate is based on the comparison between NIED moment tensors, Harvard Centroid Moment Tensor, and JMA focal mechanism catalog. In the Tottori region, since observational conditions are more favorable than those of offshore earthquakes, this 15° error might be an upper bound.

One can see in Figure 5 the excellent agreement between relocated seismicity and fault strike directions estimated by the moment tensors. Taking into consideration the estimation errors of principal axis directions of moment tensors and fits between strikes from moment tensors and hypocenter distribution, the results suggest that the scattering of the principal axes of moment tensors of aftershocks is caused by a locally complicated fault system.

We have modeled the fault structure based on the relocated aftershocks. By looking at the map view of relocated aftershocks, the strike of each fault was chosen. Then from the cross section perpendicular to the fault strike, the dip angle of each fault was estimated. These selections were done by hand. We did not use a fitting algorithm to obtain the fault plane automatically, because it was difficult to separate the earthquakes on the fault from off-fault ones. Instead, by using human eyes, we could obtain a robust fault model that convincingly explains the relocated hypocenters. The fault model is shown in Table 3 and Figure 6. We also compared the fault model with the moment tensor solutions in order to check the geometry of each fault. This comparison explicitly assures the validity of the fault-plane selection by hand. Slip directions shown in Table 3 were obtained from the moment tensor solutions.

The obtained fault traces can be classified into two groups of left-lateral faults, N145°E (faults 1, 2, 4, 5, 6) and N165°E (faults 9, 12, 13). It should be noted that the two

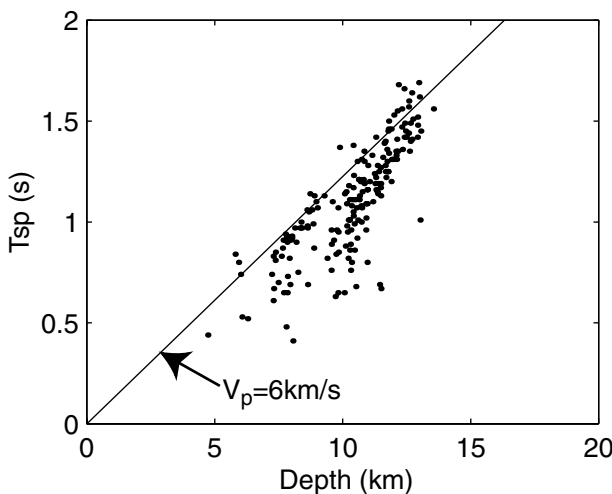


Figure 3. Correlation plot between $S-P$ times and their depths of aftershocks occurring within 3 km from station H.HINH shown in Figure 2.

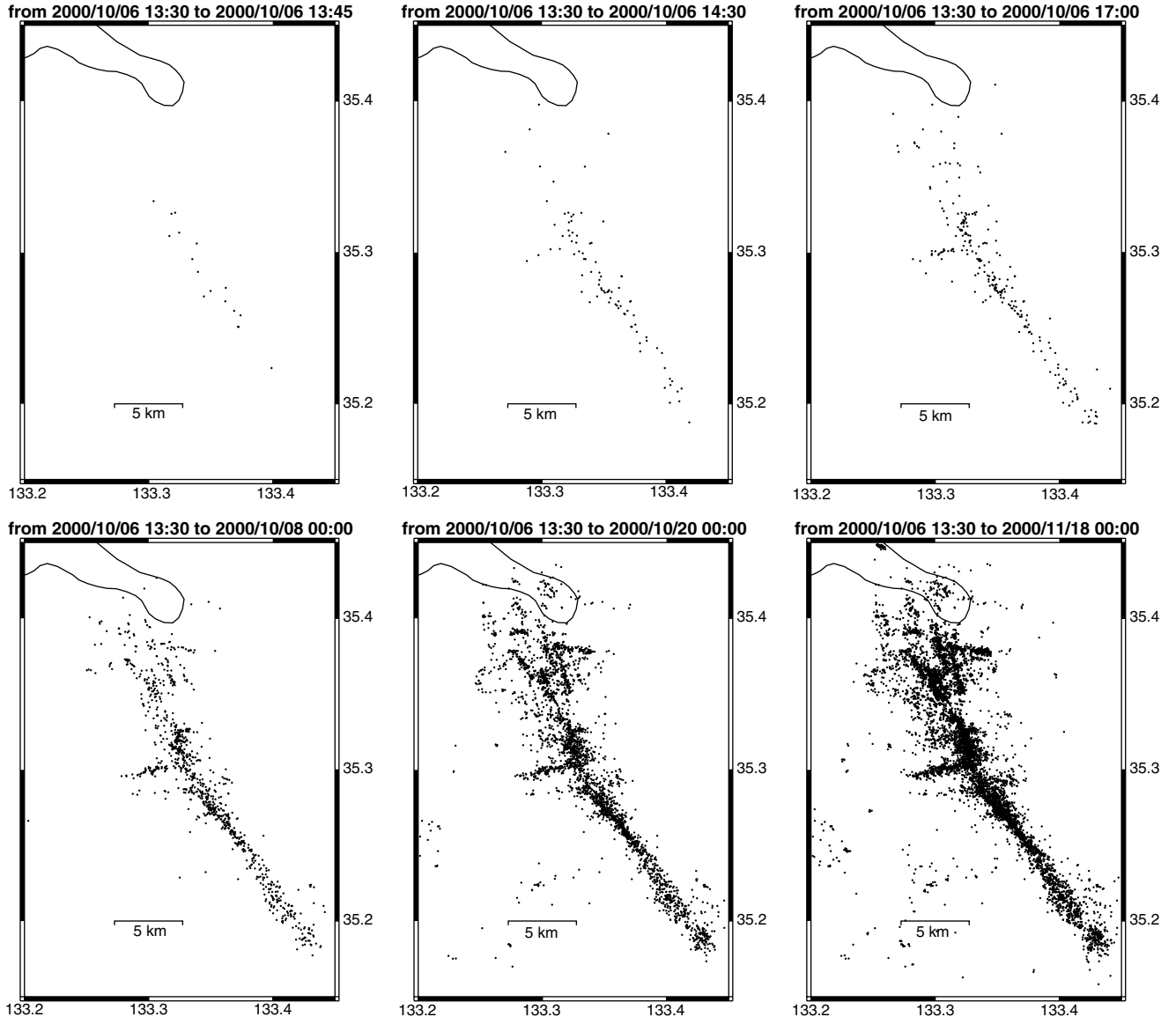


Figure 4. Snapshots of the temporal change of cumulative aftershock distribution. Aftershock activity in the western part is not shown. The time window (JST, UTC + 9) is indicated at the top of each panel.

fault groups also have associated conjugate right-lateral faults (fault 3 for the former group and faults 10 and 11 for the latter). This reflects a very complicated deformation field in this region, especially for the northern part of the fault.

Estimated Stress Field

In order to estimate the stress field, we have conducted stress tensor inversion using P - and T -axis directions of fault-plane solutions obtained from the moment tensor solutions (Fig. 5). We used the code “FMSI” developed by Gephart and Forsyth (1984) and Gephart (1990a,b). FMSI employs the grid search method to find the best-fit stress tensor that explains the fault-plane solution data set. In this

computation we used three different weighting schemes: constant, proportional to magnitude, and proportional to variance reduction. We found the result stable for all three different weighting schemes. Here we used the variance reduction weighting scheme because this weighting scheme might reflect the data quality. Following Gephart and Forsyth (1984), we evaluated the 95% confidence range of the solution as an index of error estimates. The result is shown in Figure 7 and Table 4.

Using all available fault-plane solutions, the azimuths of the $(\sigma_1, \sigma_2, \sigma_3)$ directions are $(107^\circ, 330^\circ, 200^\circ)$, respectively, where $\sigma_1, \sigma_2, \sigma_3$ stand for maximum, intermediate, and minimum principal stress, respectively. Compression is positive as conventionally used. R , which is defined as $(\sigma_1 - \sigma_2)/(\sigma_1 - \sigma_3)$, is 0.60. We call this solution ALL.

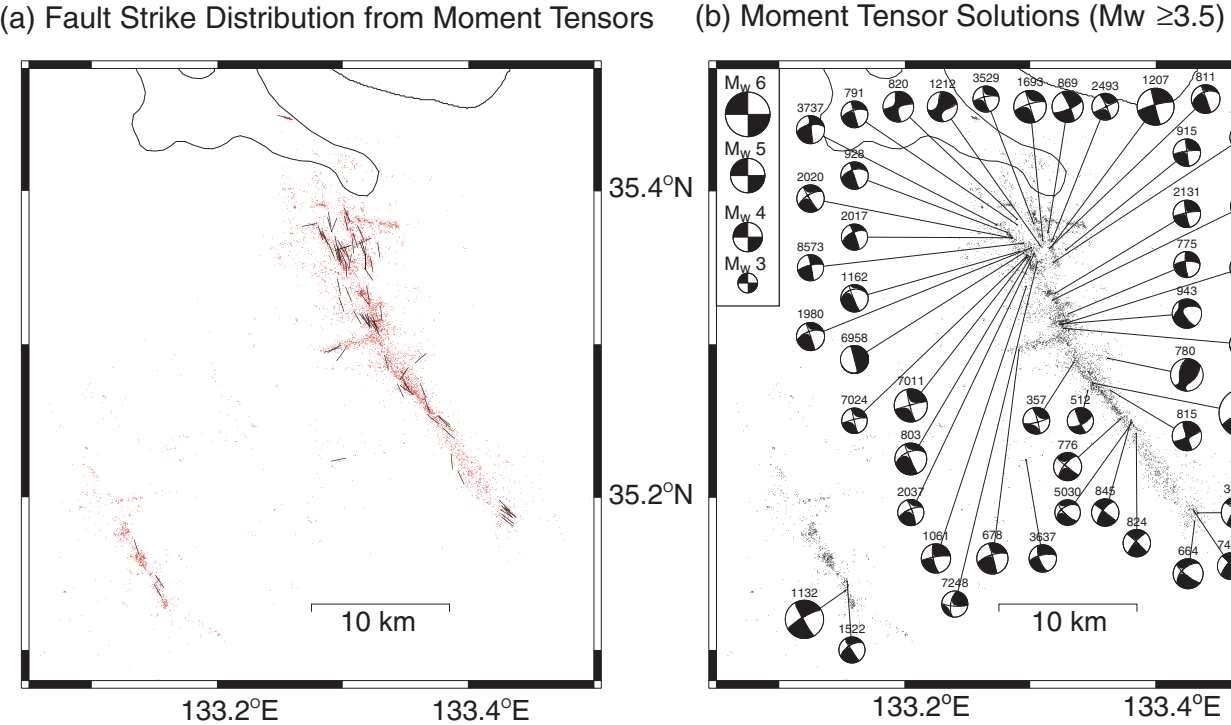


Figure 5. (a) Strike directions derived from the moment tensor analysis plotted together with the relocated aftershock distribution. (b) Estimated moment tensors of aftershocks ($M_w \geq 3.5$), plotted with relocated locations. The numbers appearing above each moment tensor correspond to the event ID in Table 2.

The 95% confidence region is quite small (less than 15°). The σ_1 direction obtained here is consistent with the tectonic stress field in this region by Tsukahara and Kobayashi (1991), who compiled focal mechanisms of shallow earthquakes and *in situ* measurements of stress in southwest Japan. Although fault strikes are scattered, the uniform stress field over the aftershock region seems to be able to explain the variation of fault-plane solutions.

However, as mentioned in the previous section, in the northern part of the aftershock region two conjugated fault pairs (the N145°E group and N165°E group) are found. Thus we also conducted the stress tensor inversion both for the northern and for the southern part in order to examine if the stress field in the entire region is homogeneous or not. We divided the whole area into two regions: north of 35.33°N and south of 35.33°N (Fig. 6). In this case, the $M_{5.1}$ aftershock and its aftershocks occurring in the western part and the mainshock were excluded.

The result is shown in Figure 7 and Table 4. In the southern part, we obtained a similar solution as that used for whole region (we call this solution South). The 95% confidence region is also very similar to that of ALL. However, in the northern part, the solution (which we call North 1) was rotated about 20° clockwise with small R . The 95% confidence region was found to be broad compared to that of South.

Since the result in the northern part does not seem to be

well constrained by the data, we introduced an additional constraint in R . We conducted two inversions assuming either $R < 0.4$ or $R \geq 0.4$. For the $R < 0.4$ case, we obtained the same solution as North 1. On the other hand, for the $R \geq 0.4$ case, we obtained the solution with the σ_1 direction of N107°E (we call this North 2), which is very similar to ALL and South. The residuals were not so different (Table 4). This result suggests that the stress field in this region can be considered homogeneous. Although the North 1 solution suggested a spatial variation of stress, its 95% confidence region is broad and a homogeneous solution (North 2) is still possible.

Since we obtained the geometry of the fault system (Fig. 6), we could compare the result with that by stress tensor inversion. For the southern part, if we assume that left-lateral faults 1, 2, 4 and right-lateral fault 3 are a conjugated pair (Fig. 6 and Table 3), the direction of principal stress axis (σ_1) is estimated at N110°E using the two conjugate strike directions. Although this is a rough estimate, this value is consistent with the stress tensor inversion result, and we could confirm that stress tensor inversion works quite well. For the northern part, left-lateral faults 9, 12, and 13 and right-lateral fault 10 are assumed to be a conjugated pair (Fig. 6 and Table 3), the principal axis direction becomes N110°E as well. This supports the second solution (North 2) of the stress tensor inversion. However, if we assume 9, 12, and 13 as left-lateral faults and 11 as a right-lateral fault,

Table 2
List of Best-Fit Double-Couple Focal Mechanism Solutions Obtained by the Moment Tensor Analysis

Event ID	Origin Time (yyyy/mm/dd JST)	Latitude (°E)	Longitude (°N)	Depth (km)	M_w	M_0 (Nm)	Strike (°)	Dip (°)	Rake (°)
2	2000/10/06 13:30:17.75	35.274630	133.349837	9.596	6.6	8.62e18	150	85	-9
357	2000/10/06 17:59:08.80	35.288127	133.334725	8.414	3.6	2.47e14	345	84	-10
372	2000/10/06 18:06:25.56	35.313668	133.324959	8.121	3.4	1.46e14	141	80	-15
474	2000/10/06 19:19:40.32	35.313025	133.325903	7.196	3.7	3.59e14	162	85	-4
512	2000/10/06 19:57:22.92	35.269775	133.345939	12.936	3.5	1.84e14	156	83	23
523	2000/10/06 20:04:50.56	35.194637	133.429028	11.342	3.4	1.26e14	136	90	6
664	2000/10/06 22:56:59.72	35.184054	133.431038	14.123	4.1	1.35e15	128	76	-38
678	2000/10/06 23:13:22.12	35.296309	133.290967	7.462	4.1	1.84e15	253	71	177
769	2000/10/07 03:58:16.38	35.328951	133.318091	9.427	3.5	2.01e14	143	90	-15
775	2000/10/07 04:50:24.78	35.319958	133.330591	6.940	3.5	1.78e14	174	79	-21
776	2000/10/07 04:56:03.38	35.250940	133.371712	9.918	3.8	5.40e14	129	86	-21
780	2000/10/07 04:59:31.14	35.290767	133.362036	6.773	4.4	3.78e15	50	51	125
791	2000/10/07 05:40:38.54	35.377999	133.289429	8.867	3.5	2.35e14	164	90	-26
801	2000/10/07 06:22:35.87	35.310494	133.326904	7.905	3.8	5.44e14	158	72	-17
803	2000/10/07 06:38:11.29	35.357096	133.300269	8.259	4.3	3.21e15	156	86	-38
811	2000/10/07 07:24:17.86	35.362598	133.315389	7.625	3.8	5.80e14	340	80	41
815	2000/10/07 07:49:30.95	35.269735	133.363957	12.339	3.9	7.59e14	159	87	10
820	2000/10/07 08:17:53.33	35.381620	133.289404	8.140	4.1	1.58e15	169	80	-4
824	2000/10/07 08:30:48.76	35.241728	133.384513	9.492	3.6	3.19e14	313	87	11
829	2000/10/07 08:57:10.55	35.297087	133.293221	6.564	3.4	1.32e14	240	49	164
845	2000/10/07 10:26:53.96	35.250391	133.380461	10.394	3.7	3.49e14	128	90	-21
868	2000/10/07 11:57:18.80	35.259998	133.367196	10.987	3.2	6.29e13	341	86	-21
869	2000/10/07 12:03:50.96	35.372974	133.314144	8.860	4.2	2.31e15	335	82	-14
871	2000/10/07 12:14:23.59	35.315999	133.317326	7.045	3.3	1.14e14	320	46	4
915	2000/10/07 16:10:38.10	35.361694	133.328687	7.509	3.7	3.61e14	172	89	-10
928	2000/10/07 17:04:31.20	35.372880	133.282137	8.306	3.7	3.71e14	161	87	-37
929	2000/10/07 17:07:55.40	35.358899	133.296867	9.422	3.3	1.06e14	351	86	20
943	2000/10/07 18:32:11.74	35.313123	133.323356	8.083	3.9	8.80e14	146	71	-40
1061	2000/10/08 06:08:21.18	35.337614	133.296834	6.757	3.9	7.79e14	169	74	-10
1063	2000/10/08 06:20:58.64	35.223246	133.386914	7.112	3.4	1.49e14	175	47	19
1132	2000/10/08 13:17:55.45	35.138822	133.152531	5.250	5.1	4.65e16	150	86	-11
1162	2000/10/08 15:47:35.57	35.360539	133.291341	8.915	3.7	3.80e14	158	83	-56
1186	2000/10/08 18:19:42.08	35.315120	133.320540	7.676	3.4	1.32e14	171	70	-2
1207	2000/10/08 20:51:17.08	35.363224	133.316536	8.224	5.0	3.11e16	165	87	-9
1212	2000/10/08 20:59:36.60	35.364335	133.308016	7.741	4.0	1.06e15	175	70	18
1218	2000/10/08 21:33:59.00	35.351880	133.323104	6.353	3.4	1.61e14	170	69	53
1308	2000/10/09 06:59:26.13	35.317521	133.311564	6.576	3.3	9.02e13	330	80	-5
1433	2000/10/09 19:24:05.36	35.270280	133.350741	11.511	3.3	9.06e13	123	57	-18
1438	2000/10/09 19:49:57.76	35.315649	133.318254	6.723	3.2	6.18e13	149	83	-22
1501	2000/10/10 02:26:16.92	35.315332	133.320247	6.661	3.4	1.36e14	334	89	36
1522	2000/10/10 04:49:18.41	35.144991	133.154224	6.735	3.5	2.19e14	146	87	-32
1650	2000/10/10 17:19:48.00	35.363969	133.298665	10.595	3.4	1.53e14	152	67	-1
1664	2000/10/10 18:22:43.92	35.345732	133.320492	8.652	3.3	1.01e14	146	85	-3
1693	2000/10/10 21:57:59.48	35.367550	133.310116	9.416	4.4	4.15e15	163	90	-14
1980	2000/10/12 03:53:31.34	35.363049	133.301009	8.177	3.8	5.59e14	252	59	179
2017	2000/10/12 06:48:51.93	35.369495	133.286027	8.804	3.5	2.34e14	338	84	30
2020	2000/10/12 07:09:00.38	35.369360	133.285579	8.482	3.7	3.62e14	147	85	-26
2037	2000/10/12 08:41:57.76	35.359049	133.303255	8.371	3.5	1.88e14	341	80	21
2131	2000/10/12 17:07:36.80	35.333341	133.320028	9.742	3.7	3.95e14	169	85	-8
2179	2000/10/12 21:48:30.10	35.332837	133.304557	8.036	3.4	1.27e14	337	71	44
2298	2000/10/13 10:44:22.01	35.270577	133.352417	9.765	3.3	1.10e14	143	79	15
2493	2000/10/14 08:01:04.97	35.367114	133.317285	10.390	3.6	2.38e14	65	88	-175
2679	2000/10/14 23:34:44.60	35.325936	133.298934	6.586	3.4	1.64e14	161	76	-31
3288	2000/10/17 06:46:56.93	35.212944	133.394295	13.949	3.3	8.75e13	155	84	33
3418	2000/10/17 19:20:30.08	35.362659	133.299406	8.961	3.4	1.37e14	252	66	178
3447	2000/10/17 22:10:49.52	35.293156	133.298665	7.194	3.4	1.29e14	216	65	155
3448	2000/10/17 22:16:59.56	35.189815	133.433577	12.126	4.3	2.84e15	309	87	18
3483	2000/10/18 01:54:29.15	35.185661	133.431641	18.239	3.3	1.10e14	129	76	-18
3529	2000/10/18 08:05:12.39	35.378939	133.302620	10.381	3.5	1.75e14	166	78	-15
3637	2000/10/18 23:39:34.00	35.224577	133.296745	7.311	3.7	3.55e14	258	69	-157

(continued)

Table 2
(Continued)

Event ID	Origin Time (yyyy/mm/dd JST)	Latitude (°E)	Longitude (°N)	Depth (km)	M_w	M_0 (Nm)	Strike (°)	Dip (°)	Rake (°)
3737	2000/10/19 08:03:41.64	35.377922	133.273405	9.145	3.8	4.90e14	259	60	176
4236	2000/10/21 07:40:38.83	35.384452	133.303548	10.024	3.4	1.66e14	156	87	-23
5030	2000/10/24 07:43:34.95	35.249040	133.381120	9.705	3.5	1.71e14	132	71	-44
5271	2000/10/25 08:03:04.46	35.189299	133.430534	11.818	3.3	1.07e14	123	81	-31
5996	2000/10/28 20:08:22.88	35.280664	133.348812	7.536	3.2	7.70e13	202	49	82
6450	2000/10/30 15:58:44.86	35.190686	133.433073	11.372	3.4	1.38e14	311	81	18
6958	2000/11/03 09:40:54.78	35.359652	133.294946	8.427	3.8	5.26e14	165	89	85
6972	2000/11/03 12:37:33.92	35.447888	133.253963	12.159	3.4	1.22e14	287	87	-17
7011	2000/11/03 16:33:54.86	35.356299	133.296818	8.759	4.4	5.23e15	165	84	-3
7024	2000/11/03 16:53:42.74	35.357943	133.297534	8.850	3.5	1.70e14	166	88	-9
7123	2000/11/03 20:20:41.52	35.349093	133.302832	7.737	3.2	7.02e13	357	78	-16
7209	2000/11/04 04:29:39.67	35.377873	133.293050	8.974	3.3	1.16e14	202	62	22
7224	2000/11/04 07:15:46.86	35.353459	133.318498	7.280	3.7	3.58e14	180	68	19
7248	2000/11/04 10:48:02.25	35.353955	133.305843	7.964	3.5	1.80e14	190	63	14
7405	2000/11/05 03:00:31.96	35.190544	133.430835	11.490	3.6	3.11e14	318	86	22
8469	2000/11/12 19:38:03.08	35.167371	133.135661	6.693	3.4	1.44e14	162	67	-7
8573	2000/11/13 18:32:25.02	35.365865	133.294784	9.064	3.5	2.31e14	348	86	15

The fault plane is chosen by comparing with the aftershock trend.

Table 3
Discrete Fault Planes Obtained from the Relocated Aftershocks and Fault Mechanism Solutions

Fault No.	Lon1 (°E)	Lat1 (°N)	Lon2 (°E)	Lat2 (°N)	Length (km)	Top (km)	Bottom (km)	Strike (°)	Dip (°)	Rake* (°)
1	133.381036	35.243979	133.436638	35.176345	9.1	6	15	146	76	-20
2	133.322846	35.304886	133.381036	35.243979	8.6	1	15	142	90	10
3	133.340950	35.309134	133.281466	35.295325	5.7	4	10	74	87	-170
4	133.312931	35.334631	133.331035	35.309134	3.3	4	16	150	90	-10
5	133.278450	35.377479	133.306465	35.345255	4.4	7	10	144	90	-20
6	133.296983	35.365792	133.312070	35.348796	2.3	7	9	144	90	-20
9	133.312070	35.380665	133.321120	35.350567	3.5	6	9	166	90	-10
10	133.337068	35.377831	133.296550	35.357647	4.3	7	11	59	86	180
11	133.303881	35.381728	133.348274	35.376061	4.1	7	10	99	90	—
12	133.322414	35.379957	133.331464	35.359417	2.4	7	10	160	90	-10
13	133.299138	35.396246	133.308188	35.363314	3.8	8	11	167	90	-10
20	133.252586	35.448299	133.259913	35.446884	0.7	11	12	103	90	20
22	133.150000	35.143413	133.159915	35.126415	2.1	4	7	334	86	10
23	133.134912	35.158639	133.154310	35.145536	2.3	5	8	129	90	-10
24	133.123274	35.179179	133.139656	35.159349	2.7	5	8	326	85	—

*In faults 11 and 24, rake angles could not be estimated because their fault planes were very clearly recognized, but no moment tensor solutions were estimated on these faults.

although 11 is not estimated the slip direction from moment tensor analysis, the principal stress direction becomes N130°E, which is consistent with the first solution (North 1) for the northern part.

Background seismicity along the aftershock region was recognized before the mainshock (Shibutani *et al.*, 2002). In the southern part, the same lineament was observed by the background seismicity, which suggests the pre-existed fault plane in the southern part. On the other hand, in the northern part, the background seismicity was vague and the pre-existing fault trace was not well developed before the mainshock.

Thus in the North 2 case, the background stress field is

considered to be homogeneous and the difference in fault orientations in the northern and southern parts is attributed to the variation of the friction on the fault. In North 1, on the other hand, the background stress field might be heterogeneous in the northern part, but the friction on the fault is rather homogeneous. As discussed in Rivera and Kanamori (2002), we could not resolve these two possibilities from the observation and additional information might be necessary.

Discussion

It should be noted that the complex pattern of aftershocks obtained in the present analysis can largely be ex-

Fault Model of the 2000 Western Tottori Earthquake Sequence

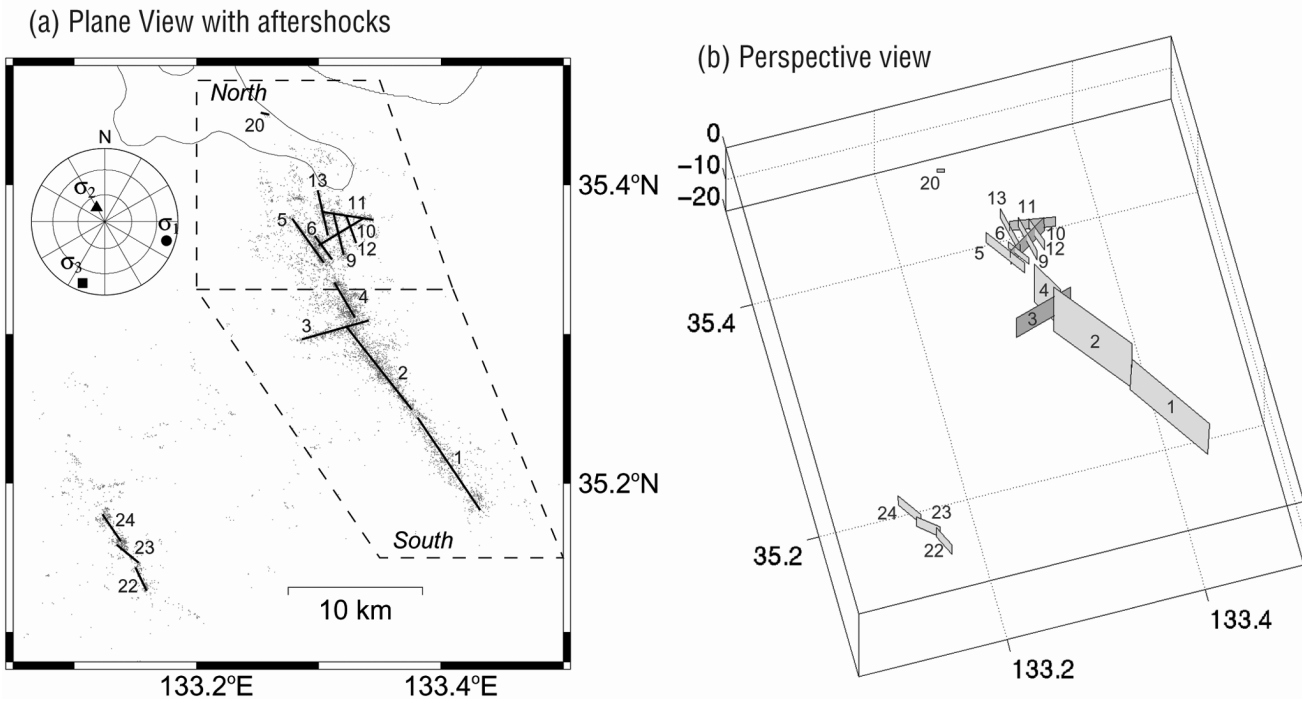


Figure 6. Fault model of the 2000 western Tottori earthquake. (a) Map view with relocated aftershocks. (b) Perspective view of inferred fault orientations. The areas named North and South surrounded by dotted lines correspond to the subset regions for the stress tensor inversion shown in Figure 7.

plained by a finite set of faults displaying brittle deformation. All the structures that can be seen from the hypocenter distribution are also consistent with the corresponding moment tensor solutions.

In the southern part, where the rupture occurred during the mainshock (Yagi and Kikuchi, 2000; Iwata and Sekiguchi, 2001), the shape of the fault is rather simple. But at the southern end, the fault is slightly twisted (Fig. 2). This might be due to the effect of the dynamic rupture. Due to the vertical gradient of the velocity structure in this region, the relative rupture velocity with respect to the shear-wave velocity becomes different between shallow and deep portions of the fault. This causes the variation of hoop stress distribution (Freund, 1990) along depth.

In the northern part, on the other hand, the fault zone appeared just after the mainshock. From the GPS measurement, most of the postseismic slip occurred in this region (Sagiya et al., 2002). This suggests that in the northern part, ductile slip started to occur just after the mainshock, and aftershocks might be caused by the stress change due to this postseismic slip. A similar phenomenon has been found in the subduction zone where postseismic slip were observed around the mainshock slip area (Yagi et al., 2001). Moreover, in the northern part, there is a possibility that the stress field might be rotated slightly clockwise. This rotation might

be caused by the postseismic slip detected by the GPS observation.

Conclusion

We relocated the aftershocks of the M_w 6.6 2000 western Tottori earthquake using the DD method and obtained a very accurate hypocenter distribution. By combining the relocated hypocenters and moment tensor solutions of aftershocks by broadband waveform inversion, we successfully resolved very detailed fault structures activated by the mainshock. The estimated fault model resolves 15 individual fault segments that are consistent with both aftershock distribution and focal mechanism solutions. Most of the faults are left-lateral strike-slip faults. We found that there are two predominant directions for left-lateral faulting striking N145°E and N165°E. Conjugate right-lateral faults are paired with both sets of left-lateral faults.

Rupture in the mainshock was principally confined to the three fault elements in the southern half of the zone, which is also where the earliest aftershocks concentrate. With time, the northern part of the zone becomes activated, which is also reflected in the postseismic deformation field determined by Sagiya et al. (2002). We conducted stress tensor inversion of aftershock focal mechanisms and found

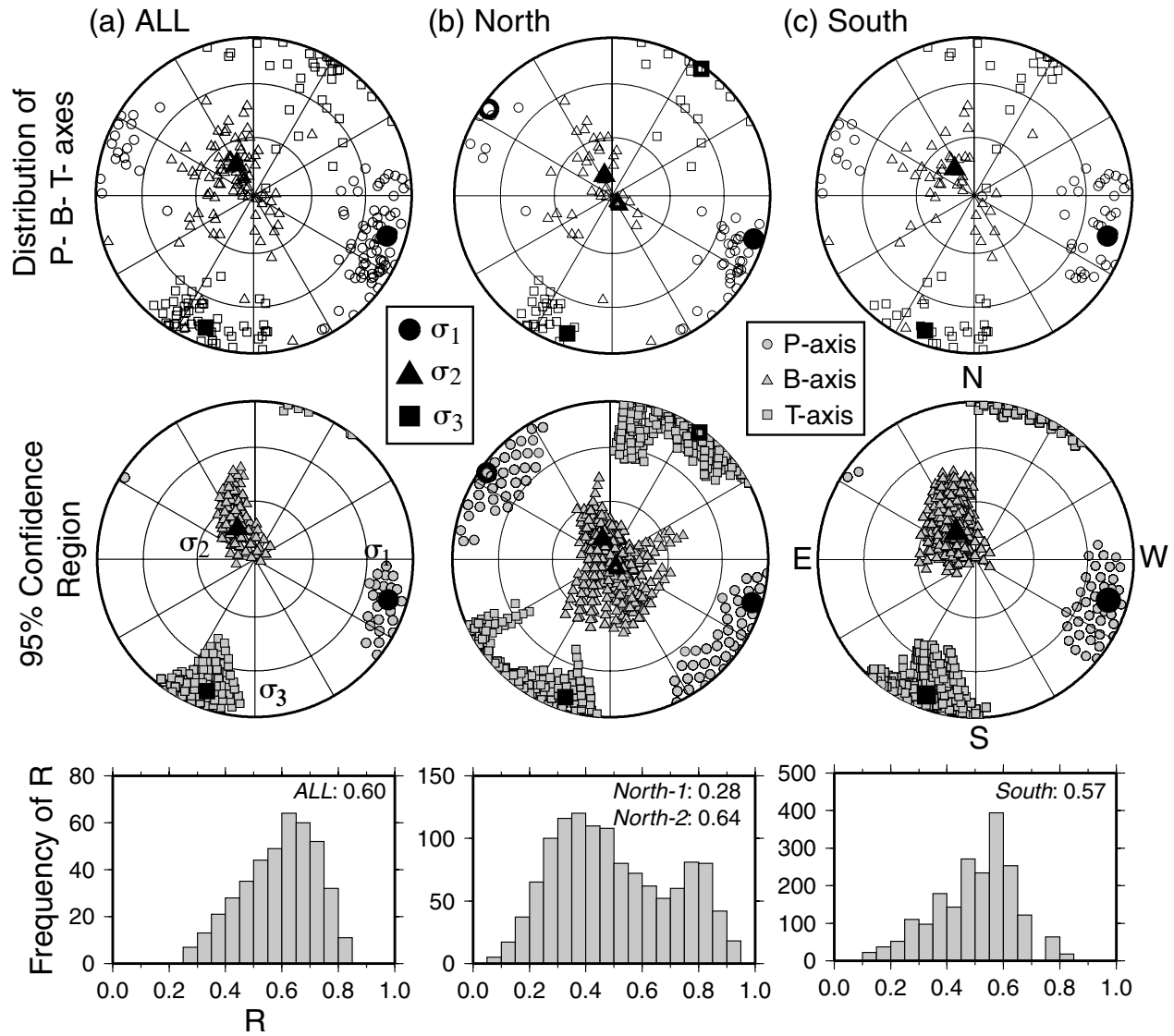


Figure 7. Result of stress tensor inversion: (a) ALL, (b) North 1 and North 2, and (c) South. Upper row shows the distribution of P - (gray circle), B - (gray triangle) and T -axes (gray square) and obtained stress axes (σ_1 , solid circle; σ_2 , solid triangle; and σ_3 , solid square). Middle row shows the 95% confidence region of the stress tensor inversion. Bottom row shows the frequency distribution of R , which belongs to the 95% confidence region. In the North column, two solutions are displayed simultaneously. Solid symbols are for the North 1 solution and open symbols are for the North 2 solution, respectively.

Table 4
Result of Stress Tensor Inversion

Region	σ_1 Plunge (°)	σ_1 Azimuth (°)	σ_2 Plunge (°)	σ_2 Azimuth (°)	σ_3 Plunge (°)	σ_3 Azimuth (°)	R	Residual (°)
ALL	13	107	72	303	12	200	0.60	4.868
North 1	7	308	83	146	2	38	0.28	4.223
North 2	7	107	79	339	9	198	0.64	4.283
South	13	107	73	324	10	200	0.57	4.739

that the maximum stress direction obtained from the stress tensor inversion is N107°E, which is consistent with other estimates of the tectonic stress field in this region. Slip on the complex fault network in the northern part can be explained either by the stress field responsible for the main-shock or by a 20° clockwise rotation of the stress field.

Acknowledgments

We would like to thank the Japan Meteorological Agency for providing us all the phase reading data for the western Tottori sequence. Reviews by Jeanne Hardebeck, associate editor, and Björn Lund and Judith Sheridan were valuable in improving the manuscript. Comments by David Schaff were helpful. GMT—the Generic Mapping Tools data processing and display software package—was used to make the figures. This work was conducted under the project “Fundamental Research on Earthquake Source and Earth Anomaly” and “Research on Earthquake Mechanism” at the National Research Institute for Earth Science and Disaster Prevention.

References

- Centroid Moment Tensor Catalog. www.seismology.harvard.edu/CMTsearch.html.
- Fukuyama, E., and D. S. Dreger (2000). Performance test for automated moment tensor determination system by using synthetic waveforms of the future Tokai earthquake, *Earth Planets Space* **52**, 383–392.
- Fukuyama, E., M. Ishida, D. S. Dreger, and H. Kawai (1998). Automated seismic moment tensor determination by using on-line broadband seismic waveforms, *Zisin (J. Seismol. Soc. Jpn.) Ser. 2*, **51**, 149–156 (in Japanese with English abstract).
- Fukuyama, E., M. Ishida, S. Horuchi, H. Inoue, S. Hori, S. Sekiguchi, T. Eguchi, A. Kubo, H. Kawai, H. Murakami, S. Yamamoto, and K. Nonomura (2001a). NIED seismic moment tensor catalogue January–December, 2000, *Technical Notes of the National Research Institute for Earth Science and Disaster Prevention* **217**, 1–131.
- Fukuyama, E., A. Kubo, H. Kawai, and K. Nonomura (2001b). Seismic remote monitoring of stress field, *Earth Planets Space* **53**, 1021–1026.
- Freund, L. B. (1990). *Dynamic Fracture Mechanics*, Cambridge U Press, New York, 563 pp.
- Gephart, J. W. (1990a). Stress and the direction of slip on fault planes, *Tectonics* **9**, 845–858.
- Gephart, J. W. (1990b). FMSI: a Fortran program for inverting fault/slickenside and earthquake focal mechanism data to obtain the regional stress tensor, *Comput. Geosci.* **16**, 935–989.
- Gephart, J. W., and D. W. Forsyth (1984). An improved method for determining the regional stress tensor using earthquake focal mechanism data: application to the San Fernando earthquake sequence, *J. Geophys. Res.* **89**, 9305–9320.
- Ichikawa, M. (1971). Reanalyses of mechanism of earthquakes which occurred in and near Japan and statistical studies on the nodal plane solutions obtained 1926–1968, *Geophys. Mag.* **35**, 207–274.
- Iwata, T., and H. Sekiguchi (2001). Substance of the earthquake faulting during the 2000 western Tottori earthquake, *SEISMO* **5**, March 2001, 5–7 (in Japanese).
- Japan Meteorological Agency (2001). *The Seismological and Volcanological Bulletin of Japan*, Japan Meteorological Agency, Tokyo.
- Joint Group for Dense Aftershock Observation of the 2000 Tottori-ken Seibu Earthquake (2001). Aftershock distribution of the 2000 Tottori-ken Seibu earthquake determined precisely by dense aftershock observation, *Abstracts 2001 Japan Earth and Planetary Science Joint Meeting*, S3-005, Tokyo, 4–8 June (CD-Rom).
- Kanamori, H. (1972). Determination of effective tectonic stress associated with earthquake faulting, the Tottori earthquake of 1943, *Phys. Earth Planet. Interiors*, **5**, 426–434.
- Kubo, A., E. Fukuyama, H. Kawai, and K. Nonomura (2002). NIED seismic moment tensor catalogue for regional earthquakes around Japan: quality test and application, *Tectonophysics* **356**, 23–48.
- NIED Seismic Moment Tensor Catalog, www.fnet.bosai.go.jp.
- Research Group for Active Faults of Japan (1991). *Active Faults in Japan*, (New Edition), Tokyo University Press, Tokyo (in Japanese).
- Rivera, L., and H. Kanamori (2002). Spatial heterogeneity of tectonic stress and friction in the crust, *Geophys. Res. Lett.* **29**, no. 6, 1088, doi 10.1029/2001GL013803.
- Sagiya, T., T. Nishimura, Y. Hatanaka, E. Fukuyama, and W. L. Ellsworth (2002). Crustal movements associate with the 2000 western Tottori earthquake and its fault models, *Zisin (J. Seismol. Soc. Jpn.) Ser. 54*, 523–534 (in Japanese with English abstract).
- Shibutani, T., S. Nakao, R. Nishida, F. Takeuchi, K. Watanabe, and Y. Umeda (2002). Swarm-like seismic activity in 1989, 1990, and 1997 preceding the 2000 western Tottori earthquake, *Earth Planets Space* **54**, 831–845.
- Tsukahara, H., and Y. Kobayashi (1991). Crustal stress in the central and western parts of Honshu, Japan, *Zisin (J. Seismol. Soc. Jpn.) Ser. 2*, **44**, 221–231 (in Japanese with English abstract).
- Waldhauser, F., and W. L. Ellsworth (2000). A double-difference earthquake location algorithm: method and application to the northern Hayward fault, California, *Bull. Seism. Soc. Am.* **90**, 1353–1368.
- Yagi, Y., and M. Kikuchi (2000). Source process of the 2000 October 6 western Tottori earthquake (preliminary report), *Newslett. Seism. Soc. Jpn.* **12**, no. 4, 9–10 (in Japanese).
- Yagi, Y., M. Kikuchi, and T. Sagiya (2001). Co-seismic slip, post-seismic slip, and aftershocks associated with two large earthquakes in 1996 in Hyuga-nada, Japan, *Earth Planets Space* **53**, 793–803.
- National Research Institute for Earth Science and Disaster Prevention
3-1 Tennodai, Tsukuba, Ibaraki, 305-0006 Japan
fuku@bosai.go.jp
kubo@bosai.go.jp
(E.F., A.K.)
- U.S. Geological Survey
345 Middlefield Road, Menlo Park, California 94025
ellsworth@usgs.gov
(W.L.E., F.W.)
- now at Lamont-Doherty Earth Observatory
Columbia University
61 Route 9W, Palisades, New York 10964
felixw@ldeo.columbia.edu
(F.W.)

Manuscript received 21 May 2002.